Pharmaceutical Sciences and Drug Design
ISSN: 3062-4428
2025, Volume 5, Page No: 114-134

Available online at: www.galaxypub.co/page/journals

Galaxy Publication

Semaglutide's Impact on Kidney Health in Obese Mice: A Metabolomics Study

Johanna Eriksson[1]*, Maja Lindgren[1]

[1]Department of Biotechnology, Faculty of Medicine, Uppsala University, Uppsala, Sweden.

***E-mail** ✉ johanna.eriksson.se@gmail.com

Received: 12 April 2025; **Revised:** 01 August 2025; **Accepted:** 02 August 2025

ABSTRACT

Semaglutide, a novel long-acting glucagon-like peptide-1 (GLP-1) analogue, has demonstrated therapeutic benefits in renal diseases; however, its specific effects on kidney metabolism in the context of obesity remain unclear. This study aimed to investigate the renoprotective effects of semaglutide and its underlying metabolic regulatory mechanisms in obesity-associated kidney injury. Male C57BL/6J mice were assigned to control and obesity groups, with the latter receiving a high-fat diet and treatment with or without semaglutide (30 nmol/kg/day). Blood biochemical parameters were measured, and kidney damage was assessed using Periodic Acid-Schiff staining and electron microscopy. Metabolomic profiling was performed to identify obesity-related metabolic alterations in renal tissue. Semaglutide markedly improved glucose regulation, insulin sensitivity, and renal injury in obese mice. A total of 377 significantly altered metabolites ($P < 0.05$) were identified. Notably, semaglutide modulated metabolites linked to oxidative stress and inflammation, including nicotinamide adenine dinucleotide (NAD+) and adenosine, which have not been previously reported in obesity-related kidney injury. Pathway enrichment analysis highlighted alterations in phospholipid and lysophospholipid metabolism, purine metabolism, NAD+ metabolism, and insulin resistance-associated pathways, suggesting potential targets for therapeutic intervention.This study provides the first metabolomics-based insight into the renoprotective mechanisms of semaglutide in obese mice. The discovery of metabolites such as NAD+ and adenosine as semaglutide targets represents a novel finding in obesity-related kidney injury, supporting semaglutide as a potential treatment for obesity-associated renal disorders.

Keywords: Kidney, Semaglutide, Glucagon-like peptide-1, Obesity, Metabolomics

How to Cite This Article: Eriksson J, Lindgren M. Semaglutide's Impact on Kidney Health in Obese Mice: A Metabolomics Study. Pharm Sci Drug Des. 2025;5:114-34. https://doi.org/10.51847/5wHbT71L9K

Introduction

Obesity has emerged as a major global public health concern and is strongly associated with an increased risk of cardiovascular diseases, diabetes mellitus, and other chronic conditions with high mortality rates [1–3]. A high body mass index (BMI) is recognized as an independent risk factor for the development and progression of chronic kidney disease (CKD) [4] and can directly contribute to obesity-related glomerulopathy (ORG) [5, 6]. As obesity prevalence rises, ORG incidence has also increased. Histologically, ORG is characterized by mesangial expansion and glomerular hypertrophy, with or without secondary focal segmental glomerulosclerosis observed under light microscopy, while electron microscopy reveals widened foot processes and reduced podocyte density [1, 3, 6]. Podocyte injury is considered a hallmark of ORG and plays a critical role in its progression [5, 6], though the precise pathophysiological mechanisms remain complex and incompletely understood. Therefore, identifying early intervention targets for ORG prevention and treatment is of significant importance.

Dipeptidyl peptidase-4 (DPP-4) inhibitors have been associated with a reduced risk of renal function decline in patients with type 2 diabetes and demonstrate protective effects against renal complications [7]. Glucagon-like peptide-1 (GLP-1), an intestinal hormone secreted by L-cells, regulates insulin secretion, appetite, and body weight, and can inhibit hyperglycemia-induced autophagy while reducing free fatty acid levels [8, 9]. GLP-1 concentrations are significantly reduced in patients with diabetic peripheral neuropathy and atherosclerosis [10–12]. Liraglutide, an acylated GLP-1 analogue, is approved for once-daily treatment of diabetes and obesity [9–

14]. Semaglutide is a newer GLP-1 analogue with enhanced albumin-binding affinity and a prolonged half-life of 165 hours, enabling once-weekly dosing [15–17]. Current research on semaglutide primarily focuses on cardiovascular disease and non-alcoholic fatty liver disease [16, 18–20], whereas its renoprotective effects and underlying mechanisms remain unclear.

Metabolomics offers a systems-level approach to comprehensively profile metabolic changes within an organism and has been widely applied in disease diagnosis, prognosis, and evaluation of therapeutic efficacy [21, 22]. Analytical techniques such as nuclear magnetic resonance (NMR), gas chromatography-mass spectrometry (GC-MS), and liquid chromatography-mass spectrometry (LC-MS) are commonly used in metabolomic studies [23]. Recent studies indicate that combined plasma and urine metabolite profiles can predict macroalbuminuria development in diabetic patients [21–24]. To date, no studies have examined the metabolic-level mechanisms by which semaglutide acts on ORG. Thus, metabolomics may provide novel insights into the renoprotective effects of semaglutide.

This study aimed to assess the renal protective effects of semaglutide in high-fat diet (HFD)-induced obese mice. By integrating untargeted metabolomics with conventional clinical chemistry, histology, and biological analyses, we sought to identify key metabolic biomarkers and pathways involved in its therapeutic action.

Materials and Methods

Ethical statement

All animal experiments were performed in accordance with institutional guidelines and were approved by the Animal Care and Treatment Committee of Hebei General Hospital (Shijiazhuang, China).

Chemicals and reagents

Semaglutide was purchased from Novo Nordisk A/S. Kits for serum creatinine (Scr), uric acid (UA), triglycerides (TG), total cholesterol (TC), high-density lipoprotein (HDL), low-density lipoprotein (LDL), superoxide dismutase (SOD), and malondialdehyde (MDA) were obtained from Nanjing Jiancheng Bioengineering Institute (Nanjing, China). Mouse insulin and microalbumin (MAU) ELISA kits were purchased from Wuhan Ilerite Biotechnology Co., Ltd. (Wuhan, China), while mouse interleukin-1β (IL-1β), interleukin-6 (IL-6), and tumor necrosis factor-α (TNF-α) kits were acquired from Hangzhou Lianke Biotechnology Co., Ltd. (Hangzhou, China).

Animals and experimental design

Six-week-old male C57BL/6J mice were obtained from Hebei Invivo Biological Technology Co., Ltd. (Shijiazhuang, China) and housed under standard conditions (22 ± 1°C, 55 ± 15% humidity, 12-hour light/dark cycle) with free access to water. After a 1-week acclimation, 10 mice were fed a normal-fat diet (NFD, 10% calories from fat) and 18 mice were fed a high-fat diet (HFD, 60% calories from fat) for 13 weeks [13, 18, 25]. Mice with body weight exceeding 20% of the NFD control were classified as obese [13, 18, 25]. After confirming successful obesity modeling, two mice from each group were randomly selected for glomerular pathology assessment. The remaining mice were divided into three groups: NFD (n = 8), HFD (n = 8), and HFD + semaglutide (HFDS, n = 8). HFDS mice received daily subcutaneous injections of semaglutide (30 nmol/kg/day) for 13 weeks. Body weight was recorded weekly, and glucose tolerance tests were performed after treatment. Urine samples were collected to measure urinary albumin/creatinine ratio (UACR). At the end of the experiment, mice were anesthetized with chloral hydrate (300 mg/kg), and kidneys were rapidly harvested. Lee's index was calculated using the formula: Lee's index = (body weight (g) × 1000) $^{(1/3)}$ / body length (cm) [25]. Perirenal and periepididymal fat were collected to calculate the abdominal fat index = (perirenal fat + periepididymal fat) / body weight [13]. Portions of the kidneys were reserved for metabolomics and histopathological analysis. The experimental workflow is summarized in **Figure 1**.

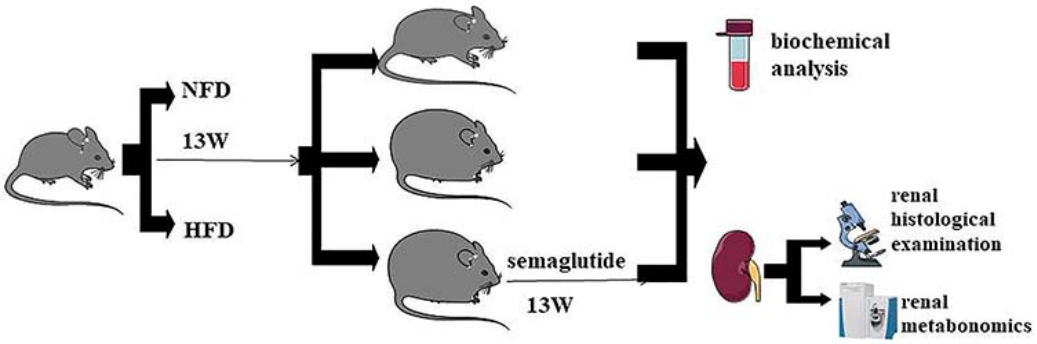

Figure 1. Flow chart of experimental design

Intraperitoneal glucose tolerance test (IPGTT)

IPGTTs were conducted after a 6-hour fast. Mice received an intraperitoneal injection of glucose at 2 mg/g body weight. Blood glucose was measured from the tail vein at 0, 15, 30, 60, 90, and 120 minutes post-injection, and the area under the curve (AUC) from 0 to 120 minutes was calculated using GraphPad Prism v.9.2 (GraphPad Software, La Jolla, CA, USA). Insulin resistance and sensitivity were evaluated using the homeostasis model assessment of insulin resistance (HOMA-IR) and the quantitative insulin sensitivity check index (QUICKI), calculated as follows: HOMA-IR = (fasting plasma glucose (mg/dL) × fasting plasma insulin (ng/mL)) / 405; QUICKI = 1 / [log(INS0) + log(G0)], where INS0 is fasting insulin (μU/mL) and G0 is fasting glucose (mg/dL) [9, 14, 18, 26, 27].

Biochemical analysis

At study completion, blood was collected immediately after ocular extraction. Serum levels of creatinine (Scr), uric acid (UA), total cholesterol (TC), triglycerides (TG), high-density lipoprotein (HDL), low-density lipoprotein (LDL), urinary creatinine (Ucr), and microalbumin (MAU) were measured using commercial kits according to the manufacturers' instructions. Urinary albumin-to-creatinine ratio (UACR) was calculated from MAU and Ucr. Creatinine clearance (Ccr) was determined as: Ccr = (Ucr × urine volume per minute) / Scr × 100% (mL/min) [8].

Renal histological examination

Light microscopy

Kidney tissues (3 mm thick) were fixed in 4% paraformaldehyde phosphate buffer for 48 hours at room temperature, dehydrated through graded ethanol (70–100%), cleared in xylene, and embedded in paraffin. Sections (5 μm) were stained with hematoxylin and eosin (HE) and periodic acid-Schiff (PAS). Glomerular diameter and tubular injury were quantified as previously described. Twenty images of maximal glomerular profiles with vascular and/or urinary poles were randomly selected and measured using Image-Pro Plus 6.0 software (Media Cybernetics, USA) [8, 28]. Tubular injury was assessed in 20 random fields (×200 magnification), scoring vacuolar degeneration or necrosis semi-quantitatively: <25%, 26–50%, 51–75%, and >75% of the field were scored as 1, 2, 3, and 4, respectively [6].

Oil red O staining

Frozen kidney sections (5 μm) were fixed in 4% paraformaldehyde, incubated with Oil Red O (KeyGen Biotech Co. Ltd., Nanjing, China) at 37°C for 20 minutes, washed with PBS, and counterstained with hematoxylin. The lipid droplet-positive area percentage was quantified [5, 6].

Transmission electron microscopy (TEM)

Kidney samples were cut into 1 mm^3 cubes, fixed in 2.5% glutaraldehyde (0.1 M phosphate buffer), washed in PBS, and post-fixed in 1% osmium tetroxide for 2 hours. Samples were dehydrated through ethanol, infiltrated with a 1:1 mixture of anhydrous acetone and embedding agent, sectioned into ultrathin slices (100 nm), mounted on copper grids, and stained with tannic acid and lead solution [5, 6].

Renal metabolomics analysis

Sample preparation for untargeted metabolomics

Approximately 30 mg of kidney tissue was placed in a 1.5 mL Eppendorf tube, stored at −20°C for 2 minutes, and ground at 60 Hz for 2 minutes. Samples were extracted ultrasonically in an ice-water bath for 10 minutes and centrifuged at 13,000 rpm for 10 minutes at 4°C. Supernatants were reconstituted in 300 μL methanol-water (1:4, v/v), sonicated for 3 minutes, centrifuged again at 13,000 rpm for 10 minutes at 4°C, filtered (0.22 μm), and stored at −80°C for LC-MS analysis. Quality control (QC) samples were prepared by pooling aliquots from all samples [25, 29].

LC-MS conditions

Metabolomic profiling was performed on a Waters ACQUITY UHPLC system coupled with a QE High Definition Mass Spectrometer (Waters, USA). Separation was achieved on an ACQUITY UHPLC HSS T3 column (100 mm × 2.1 mm, 1.8 μm) at 40°C with a 5 μL injection volume. Mobile phases were 0.1% formic acid in water (A) and acetonitrile (B), at a flow rate of 0.35 mL/min. The gradient ramped from 5% to 100% B over 12 minutes, held at 100% B for 2 minutes, and returned to initial conditions. ESI source operated in positive and negative modes, and samples were kept at 4°C during analysis [25, 29].

Data processing and pattern recognition

Data alignment was performed using Application Manager (Waters), generating a matrix of retention time, m/z, and peak intensity. Multivariate analyses, including principal component analysis (PCA) and orthogonal partial least squares-discriminant analysis (OPLS-DA), were used to identify patterns. S-plots and variable importance in projection (VIP) scores from OPLS-DA were used to select potential biomarkers. Model quality was evaluated using R^2Y and Q^2 parameters. Statistical significance was assessed using Student's t-test in SPSS v21. Identified metabolites were annotated by matching accurate mass, fragmentation patterns, and isotopic distributions against HMDB, Lipidmaps (v2.3), METLIN, and a proprietary database from Shanghai Lu-Ming Biotech. Relevant metabolic pathways were verified using the KEGG database (http://www.genome.jp/kegg/pathway.html).

Correlation analysis

Pearson correlation was used to evaluate associations between clinical and pathological parameters (e.g., UACR, Scr, glomerular diameter) and the identified metabolites.

Statistical analysis

Normality of the data was assessed using the Shapiro–Wilk test and QQ plots. Parametric tests were applied to normally distributed data, while non-parametric tests were used for data that violated normality assumptions. Results are presented as means ± standard deviation (SD). Comparisons between two groups were performed using Student's t-test for normally distributed data. For comparisons among multiple groups, one-way analysis of variance (ANOVA) or the non-parametric Kruskal–Wallis test was employed, followed by Bonferroni post hoc corrections where appropriate. A P-value <0.05 was considered statistically significant. Metabolomics data were analyzed using the aforementioned software and statistical approaches.

Results and Discussion

Modeling evaluation

After 13 weeks of a high-fat diet (HFD), mice were assessed for obesity modeling using body weight, Lee's index, and glomerular diameter. As illustrated in **Figure 2**, mice on HFD exhibited significant weight gain starting from the second week, with the difference becoming more pronounced over time. By the end of the modeling period, body weight in the HFD group was markedly higher than in the control group (43.35 ± 3.23 g vs 28.01 ± 1.80 g, $P < 0.001$). Histological analysis revealed glomerular enlargement, mesangial matrix proliferation, and tubular epithelial cell necrosis in HFD mice. PAS staining confirmed that the glomerular diameter in the HFD group was significantly larger than in the NFD group (68.57 ± 4.84 μm vs 57.30 ± 3.03 μm, $P = 0.001$) **(Figures 3a and 3b)**. Additionally, the Lee's index of HFD mice was significantly higher than that of controls (3.40 ± 0.75 vs 3.14 ± 0.56, $P < 0.001$) **(Figure 3c)**, confirming successful establishment of the obesity model.

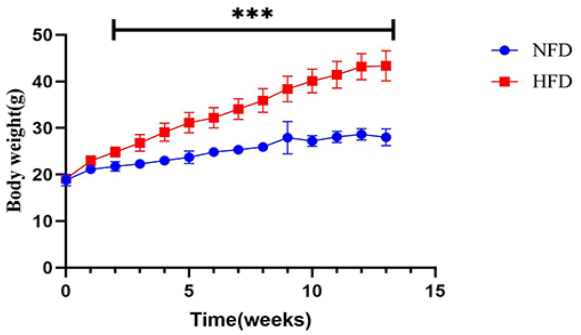

Figure 2. Body weight comparison between NFD and HFD mice. ***P < 0.001 versus the NFD group.

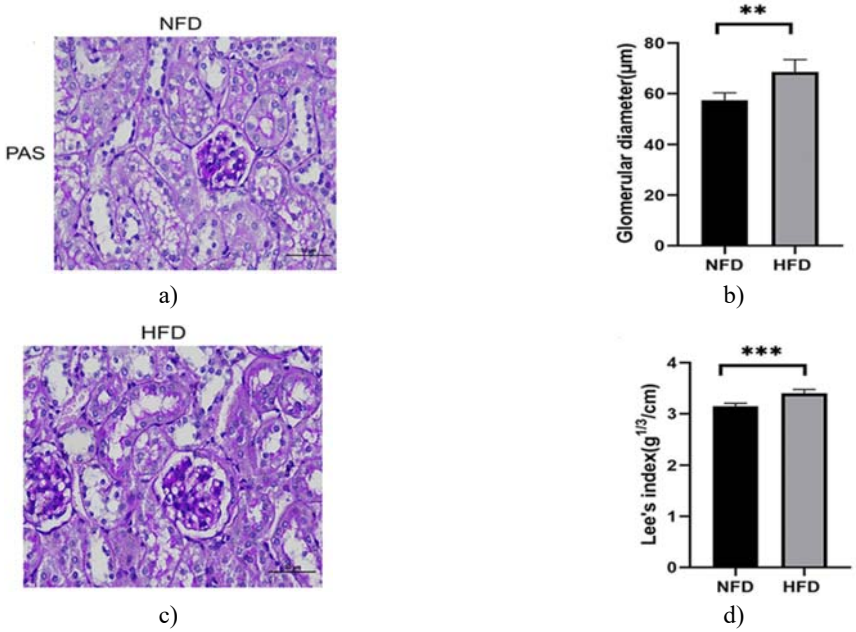

Figure 3. Lee's index and glomerular diameter in HFD and NFD mice. (a) Representative PAS-stained kidney sections (×400 magnification). (b) Quantification of glomerular diameter. (c) Lee's index of mice. **P < 0.01, ***P < 0.001 versus NFD group.

Effect of semaglutide on body weight and body composition

During semaglutide treatment, body weight in the HFDS group decreased significantly, whereas the HFD group continued to gain weight (NFD: 27.98 ± 1.23 g; HFD: 44.17 ± 3.92 g; HFDS: 29.23 ± 1.02 g; P < 0.001**) (Figure 4).** Post-mortem analyses revealed statistically significant differences between all groups. As shown in **Figures 5 and 6**, HFD feeding increased Lee's index, abdominal fat index, and right kidney weight, all of which were markedly reduced following semaglutide administration, with significant differences observed.

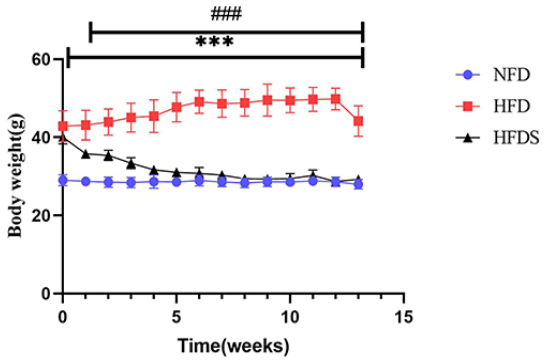

Figure 4. Effect of semaglutide on body weight. Data represent mean values for each group (n = 8 per group). ***P < 0.001 versus NFD group; ###P < 0.001 versus HFD group.

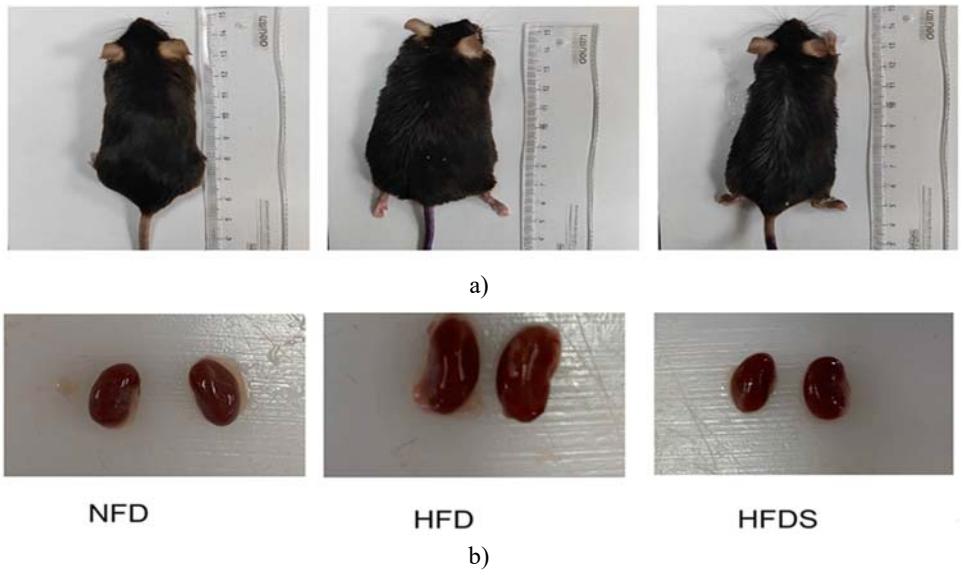

Figure 5. Effect of semaglutide on body and kidney morphology in mice. (a) Representative gross appearance of mice from each group. (b) Representative gross appearance of kidneys from each group.

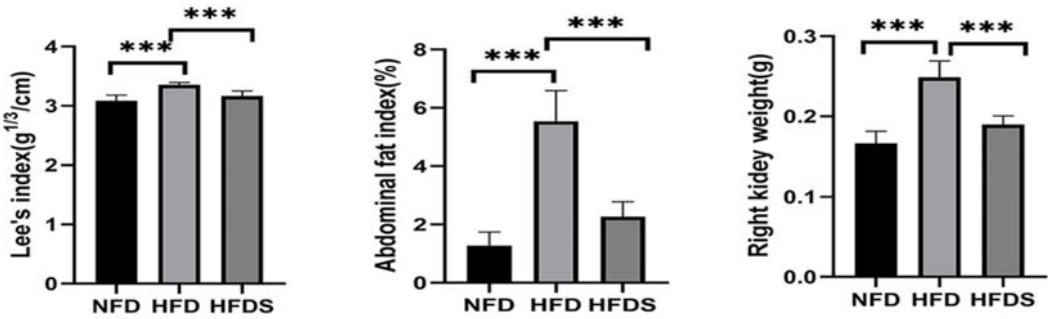

Figure 6. Effect of semaglutide on Lee's index, abdominal fat index, and right kidney weight. Data represent mean values for each group (n = 8 per group). ***P < 0.001 versus NFD or HFD group. (a) Lee's index. (b) Abdominal fat index. (c) Right kidney weight.

Effect of semaglutide on biochemical parameters and insulin resistance

To assess the impact of semaglutide on obesity-related glomerulopathy (ORG), biochemical and metabolic parameters were compared across groups **(Table 1)**. Mice in the HFD group exhibited significantly elevated levels of uric acid (UA), fasting glucose (G0), total cholesterol (TC), LDL, HDL, and UACR compared with the NFD group, reflecting metabolic dysregulation. Semaglutide treatment significantly reduced these elevated parameters, while serum creatinine (Scr) levels showed no significant differences among groups.

Table 1. Effects of Semaglutide on Biochemical Parameters

Parameters	Scr (μmol/)	Ccr (mL/min)	Ua (μmol/)	TG (mmol/L)	TC (mmol/L)	LDL (mmol/L)	HDL (mmol/L)	UACR (mg/mmol)	INS0(pg/mL)	G0(mmol/L)
NFD	60.68±9.91	(2.01±0.62)%	138.19±23.97	0.64±0.10	3.15±0.39	2.19±0.47	2.86±0.61	0.18±0.06	300.05±44.02	4.36±0.59

HFD	62.72±11.46	(3.09±0.11)%*	254.63±42.34***	0.93±0.13***	8.36±1.23***	6.79±1.37***	6.94±1.18***	0.83±0.15***	411.69±143.500	7.86±1.65***
HFDS	61.37±9.66	(2.23±0.40)%	172.83±19.04###	0.72±0.16##	5.84±0.45###	4.78±0.45###	4.56±0.86###	0.38±0.13###	174.86±59.92###	6.74±1.52

Notes: *P < 0.05, ***P < 0.001 versus NFD; ##P < 0.01, ###P < 0.001 versus HFD.
Abbreviations: Scr, serum creatinine; UA, uric acid; TG, triglyceride; TC, total cholesterol; HDL, high-density lipoprotein; LDL, low-density lipoprotein; Ccr, creatinine clearance; UACR, urinary albumin/creatinine ratio; INS0, fasting plasma insulin; G0, fasting blood glucose.

HFD-fed mice exhibited higher fasting blood glucose and fasting insulin compared with NFD controls; however, fasting glucose levels in HFD mice did not reach the threshold for diabetes diagnosis. Semaglutide treatment significantly lowered fasting insulin, though fasting glucose remained unchanged. The area under the glucose tolerance curve (AUC) was elevated in HFD mice relative to NFD controls, and semaglutide effectively reduced the AUC (NFD: 1619 ± 78.59; HFD: 2667 ± 119.8; HFDS: 1626 ± 130.9) **(Figure 7).** Indices of insulin resistance (HOMA-IR) and insulin sensitivity (QUICKI) confirmed impaired insulin signaling in HFD mice, which was ameliorated by semaglutide treatment, indicating improvement of HFD-induced insulin resistance **(Figure 7)**.

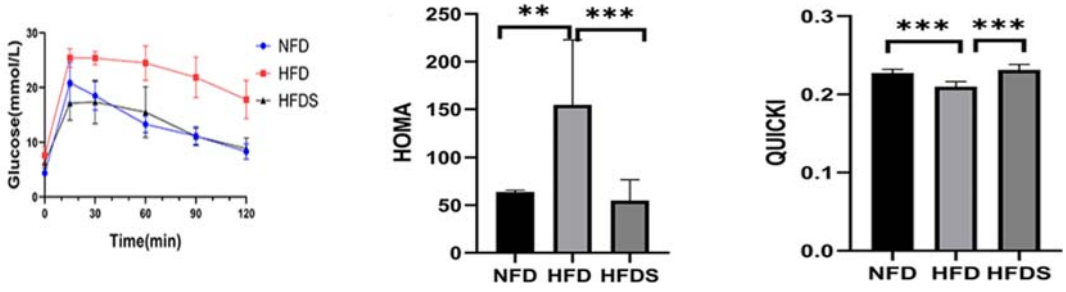

a) b) c)

Figure 7. Effect of semaglutide on glucose homeostasis and insulin resistance. Data represent mean values for each group (n = 8 per group). **P < 0.01, ***P < 0.001 versus NFD or HFD group. (a) Blood glucose levels at different time points. (b) HOMA-IR index. (c) QUICKI index.

Effect of semaglutide on renal histopathology

Light microscopy revealed that HFD-fed mice exhibited glomerular enlargement, mesangial expansion, and vacuolated renal tubular epithelial cells. Focal lymphocyte infiltration was also observed, although Masson staining showed no obvious renal interstitial fibrosis. Compared with NFD mice, HFD mice demonstrated expanded mesangial areas and increased glomerular volume. Semaglutide treatment markedly alleviated glomerular and tubular injury **(Figure 8)**. Oil Red O staining indicated substantial lipid accumulation in HFD kidneys, which was significantly reduced following semaglutide administration **(Figure 9)**.

Transmission electron microscopy (TEM) revealed swollen podocytes with irregular shapes and flattened foot processes in HFD mice, along with widened or fused foot processes and endothelial cell detachment from the basement membrane. NFD podocytes displayed abundant rough endoplasmic reticulum (RER) and numerous mitochondria with intact cristae. In contrast, HFD mice showed reduced RER, partial RER expansion, and mitochondria with lost cristae and decreased matrix density. The basement membrane was mildly thickened in localized regions. Semaglutide treatment restored podocyte ultrastructure, including normal mitochondrial density, cristae integrity, and RER content **(Figure 10).**

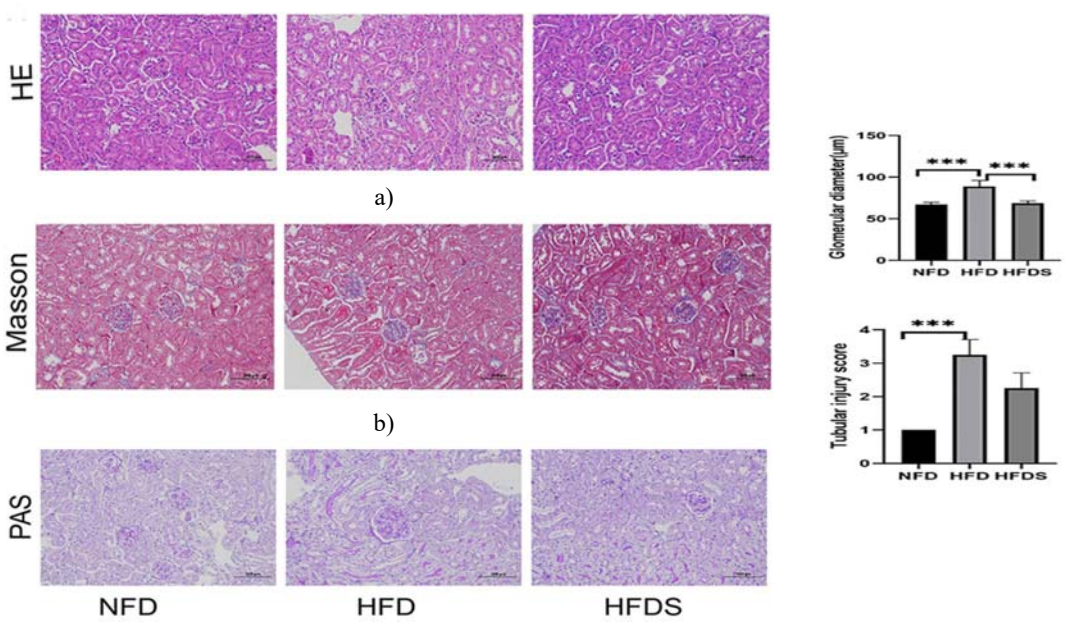

Figure 8. Semaglutide attenuated HFD-induced glomerular and tubular damage. (A) Representative HE-stained kidney sections (×200). (B) Representative Masson-stained sections (×200). (C) Representative PAS-stained sections (×200). ***P < 0.001 versus NFD or HFD group.

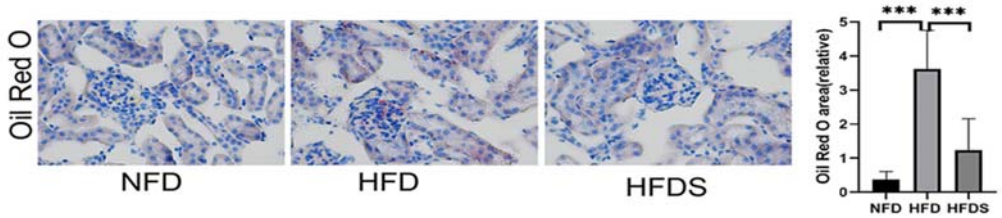

Figure 9. Semaglutide reduced lipid droplet accumulation in HFD mice as shown by Oil Red O staining (×400). ***P < 0.001 versus NFD or HFD group.

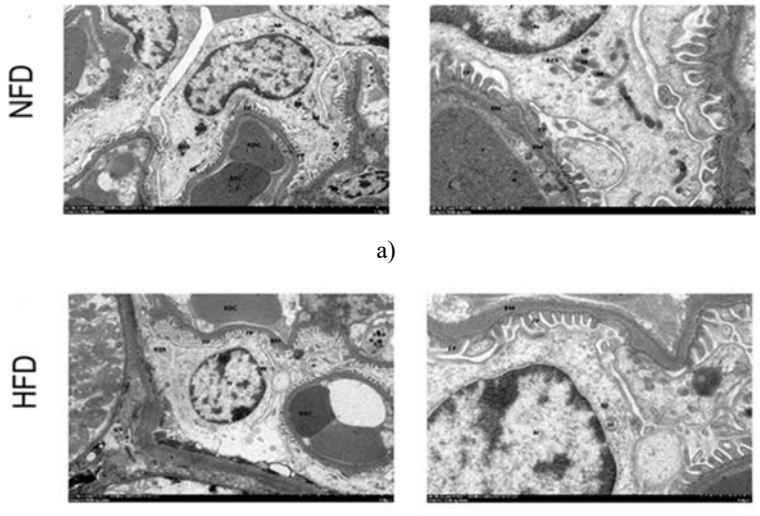

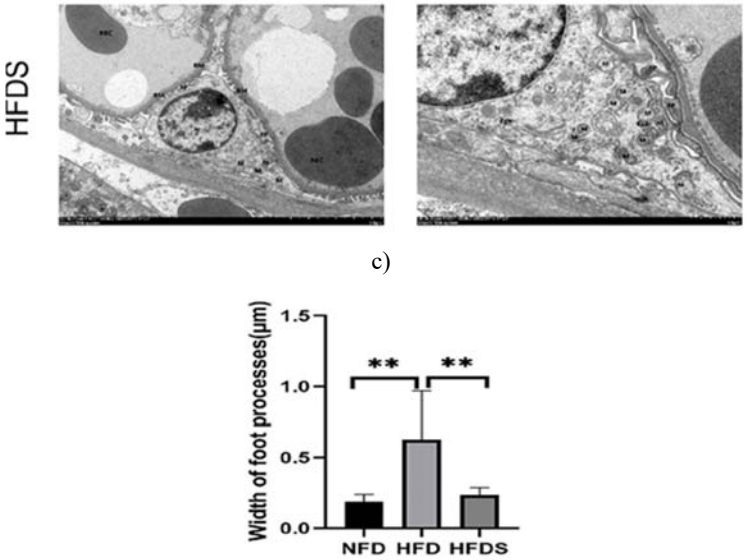

Figure 10. Semaglutide alleviated HFD-induced podocyte and mitochondrial injury. **P < 0.01 versus NFD or HFD group. (a) Representative electron microscopy images of podocytes and mitochondria in the NFD group. (b) Representative images in the HFD group. (c) Representative images in the HFDS group.

Effect of semaglutide on renal metabolomics

Multivariate analysis and LC-MS validation

To ensure reproducibility and high-quality metabolomic data, principal component analysis (PCA) and orthogonal partial least-squares discriminant analysis (OPLS-DA) were applied. PCA, an unsupervised method, visualized metabolic differences among groups, and the PCA score plots **(Figure 11)** confirmed system stability during sample analysis. Clear distinctions in metabolic profiles were observed between groups.

Using supervised pattern recognition, the OPLS-DA model was constructed to maximize group separation and identify potential biomarkers. The OPLS-DA score plot **(Figure 12)** showed clear discrimination among all groups. The model demonstrated good fit and predictive ability, with $R^2Y = 0.855$ and $Q^2 = 0.524$, indicating robustness. Each point in the S-plot represented a metabolite; points farther from the origin indicated greater influence and higher VIP values. Metabolites with VIP > 1 and P < 0.05 (t-test) were considered potential biomarkers.

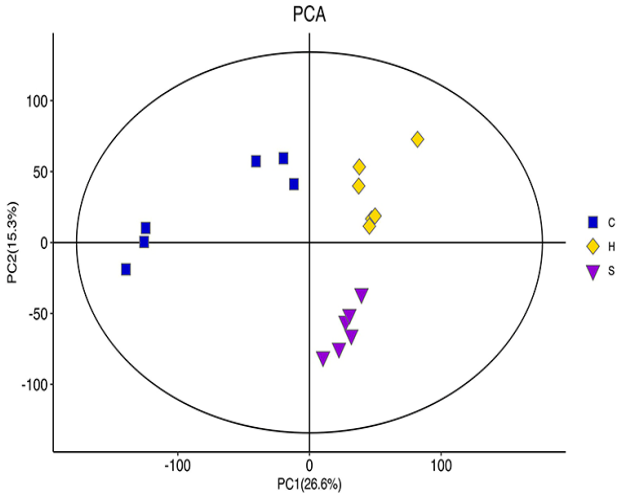

Figure 11. Principal component analysis (PCA) of untargeted renal metabolite profiles. (C) NFD group, (H) HFD group, (S) HFDS group.

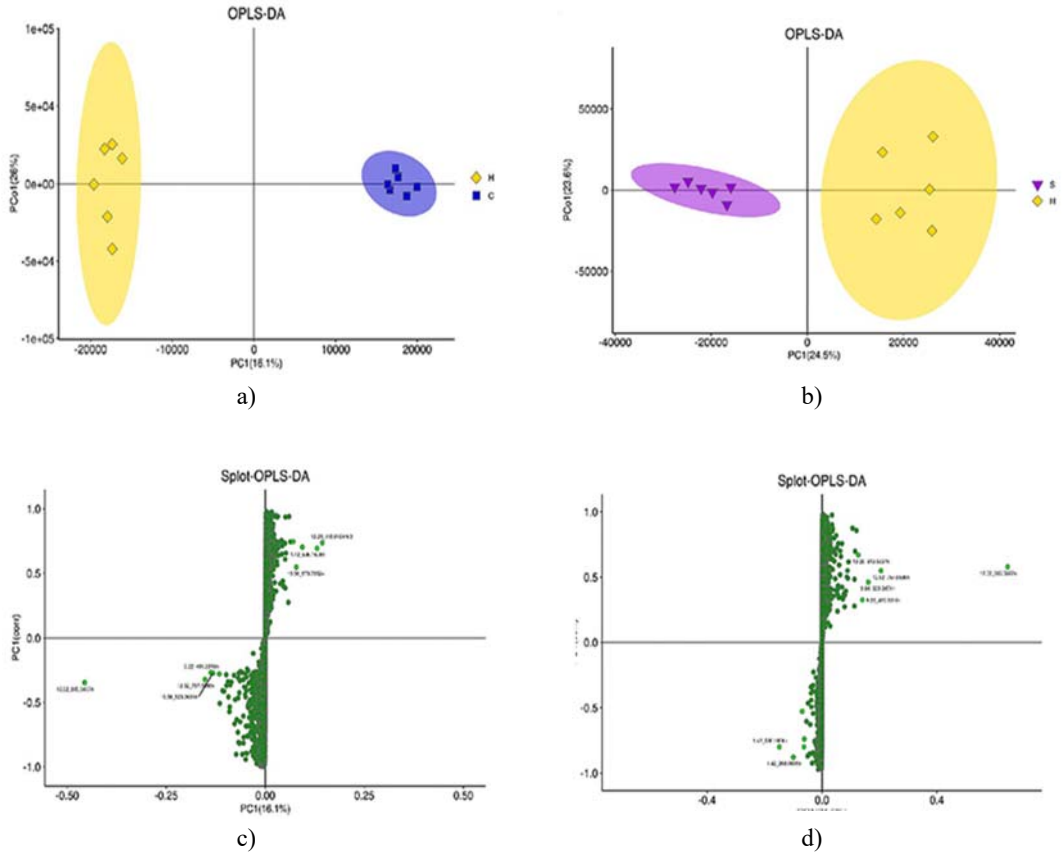

Figure 12. OPLS-DA score plots and S-plots of renal metabolic profiles. Comparisons between NFD and HFD groups (a and c) and between HFD and HFDS groups (b and d).

Identification and quantitative analysis of renal metabolites

Metabolic profiling of kidney tissues provided insights into mechanisms underlying ORG. A total of 377 statistically significant endogenous metabolites were identified ($P < 0.05$). The volcano plot **(Figure 13)** illustrates up- and down-regulated metabolites between groups. Hierarchical clustering heatmaps (**Figure 14)** depict sample relationships and differences in metabolite expression across groups.

Among these, 97 metabolites were consistently expressed across NFD, HFD, and HFDS groups. Further analysis identified 27 metabolites that were significantly up- or down-regulated in HFD mice and reversed in HFDS mice, based on VIP scores and P-values. Detailed information on these biomarkers is summarized in **Table 2**.

Table 2. Identification and the Change Trend of Metabolites

Identification	RT (Min)	Measured Mass (Da)	Mass Error (ppm)	Formular	Average (ND)	Average (HFD)	Average (HFDS)	VIP	*P*-value
1,4-beta-D-Glucan	1.42	559.15	3.54	C18H32O18	65,369,617.90	48,857,333.00	74,318,348.30	13.42	0.01
11,12-Epoxyeicosatrienoic acid	9.80	319.23	−0.11	C20H32O3	167,481.00	407,495.01	177,941.70	1.53	<0.001

Adenosine	1.27	268.10	−1.59	C10H13N5O4	1,370,252.79	919,528.25	1,359,705.27	2.13	0.02
Adenosine 3'-monophosphate	1.16	348.07	−2.05	C10H14N5O7P	386875.91	286,103.57	474,093.50	1.18	0.01
D-4'-Phosphopantothenate	1.48	322.07	−1.469	C9H18NO8P	927704.77	1,175,796.35	697,507.92	2.28	<0.001
Asymmetric dimethylarginine	0.77	203.15	−0.83	C8H18N4O2	172,720.50	307,240.01	219,296.58	1.31	0.01
Guanosine	1.39	284.10	−1.65	C10H13N5O5	577,369.50	332,028.89	698,627.17	1.64	0.003
Indoleacrylic acid	3.31	188.07	−2.13	C11H9NO2	3,975,532.01	5,725,032.90	4,028,923.94	4.64	<0.001
LysoPA (18:0/0:0)	15.402	483.27	0.36	C21H43O7P	36683.27	180,354.24	66,568.92	1.32	0.001
LysoPE (0:0/20:4(5Z,8Z,11Z,14Z))	8.72	500.28	0.07	C25H44NO7P	4728368.51	10,215,160.04	5,082,197.73	7.49	0.01
LysoPE (22:5(4Z,7Z,10Z,13Z,16Z)/0:0)	9.18	526.29	−0.66	C27H46NO7P	38161.35	782,756.87	355,441.02	3.44	<0.001
METHACHOLINE	0.89	160.13	−1.67	C8H17NO2	2,965,631.40	413,444.05	1,673,104.43	6.67	<0.001
N-arachidonoyl taurine	12.52	410.24	−0.25	C22H37NO4S	33758.13	192,106.82	103,225.09	1.57	0.0002

Nicotinamide adenine dinucleotide (NAD)	0.83	664.12	−1.55	C21H27N7O14P2	316,727.49	203,503.40	359,178.02	1.02	0.006
N-linoleoyl taurine	12.52	386.24	0.15	C20H37NO4S	106447.28	242,114.36	91,045.56	1.11	0.01
PC (22:5(4Z,7Z,10Z,13Z,16Z)/0:0)	9.38	614.35	0.27	C30H52NO7P	2910.95	515,370.32	209,872.66	2.76	0.0003
PC (O-16:0/0:0)	9.56	526.35	−0.23	C24H52NO6P	1657370.18	5,093,635.99	2,371,165.05	6.55	0.0002
PC (P-18:0/0:0)	9.88	552.37	0.471104185	C26H54NO6P	266896.67	813,718.29	342,717.88	2.53	0.0002
PE (20:5(5Z,8Z,11Z,14Z,17Z)/0:0)	9.18	544.27	−0.06	C25H42NO7P	1835805.36	4,156,406.20	2,577,357.36	5.17	0.008
PE (22:5(4Z,7Z,10Z,13Z,16Z)/0:0)	9.34	526.29	−0.46	C27H46NO7P	4910.74	735,655.88	249,850.39	3.22	<0.001
PE (O-16:0/0:0)	9.49	438.30	0.65	C21H46NO6P	55297.67	269,334.45	74,592.56	1.49	0.0002
PE (P-16:0e/0:0)	9.54	436.28	−0.15	C21H44NO6P	767813.32	1,976,051.83	745,052.29	3.39	0.006
PG (18:2(9Z,12Z)/0:0)	11.08	507.27	−0.39	C24H45O9P	690864.16	3,136,507.17	2,111,440.98	6.73	<0.001
PI (20:4(5Z,8Z,11Z,14Z)/0:0)	10.31	619.29	0.10	C29H49O12P	4097682.19	8,237,500.87	5,212,178.98	6.68	0.01

PS (16:0/0:0)	10.01	496.27	0.12	C22H44NO9P	434844.70	1,062,458.63	367,896.70	2.65	0.001
Tetrahydro-2-methyl-3-furanol	0.77	120.10	0.72	C5H10O2	113,988.31	231,696.98	74,754.58	1.43	0.002
All-trans-heptaprenyl diphosphate	9.40	699.38	2.24	C35H60O7P2	4657.89	183,331.12	85,839.12	1.65	0.0002

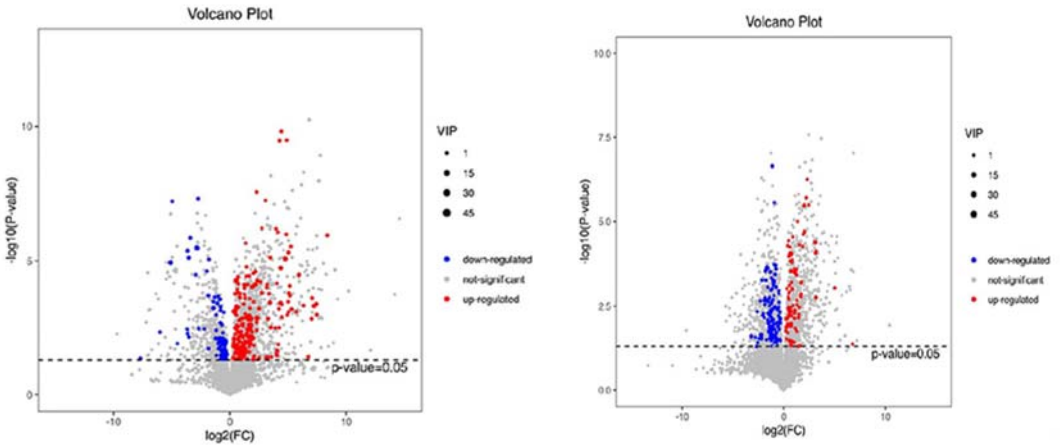

a) b)

Figure 13. Volcano plots of renal metabolic profiles. Comparison between NFD and HFD groups (a) and between HFD and HFDS groups (b). Red dots indicate significantly up-regulated metabolites, blue dots indicate significantly down-regulated metabolites, and gray dots represent non-significant metabolites.

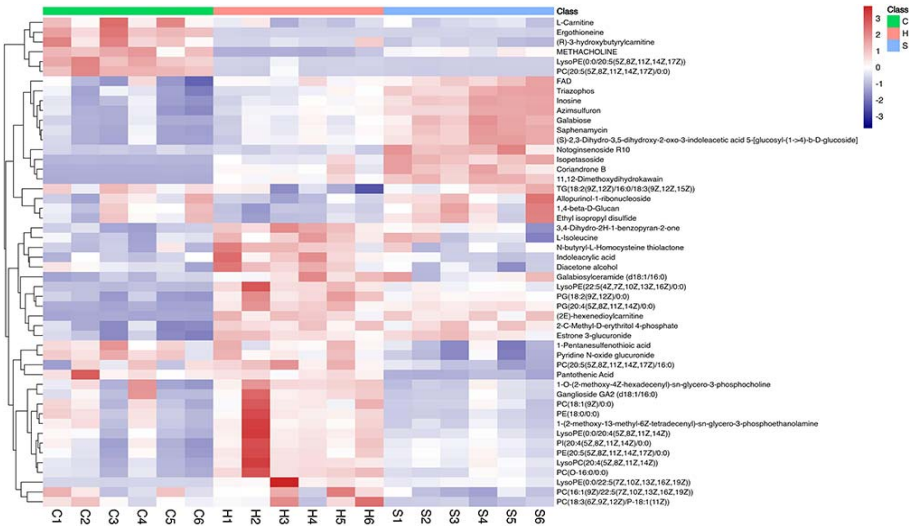

Figure 14. Hierarchical clustering heatmap of renal metabolites. (C) NFD group, (H) HFD group, (S) HFDS group. The x-axis represents sample names, and the y-axis represents differential metabolites. Colors from blue to red indicate increasing metabolite abundance.

Disturbed metabolic pathways

Integrating multivariate analysis, metabolic pathways with $P < 0.05$ were considered significantly affected. In obese mice, major disturbed pathways included purine metabolism, ABC transporters, renin secretion, FoxO signaling, aminoacyl-tRNA biosynthesis, and cGMP-PKG signaling. Following semaglutide treatment, altered pathways involved purine metabolism, pantothenate and CoA biosynthesis, beta-alanine metabolism, and vitamin digestion and absorption. KEGG database analysis highlighted pathways such as lysophospholipid metabolism, purine metabolism, NAD+ metabolism, and insulin resistance-related metabolism. A bubble plot **(Figure 15)** illustrated pathway enrichment, where the x-axis represents the rich factor (number of significantly altered metabolites / total metabolites in the pathway), colors from green to red indicate decreasing P-values, and larger points indicate a greater number of metabolites enriched in the pathway.

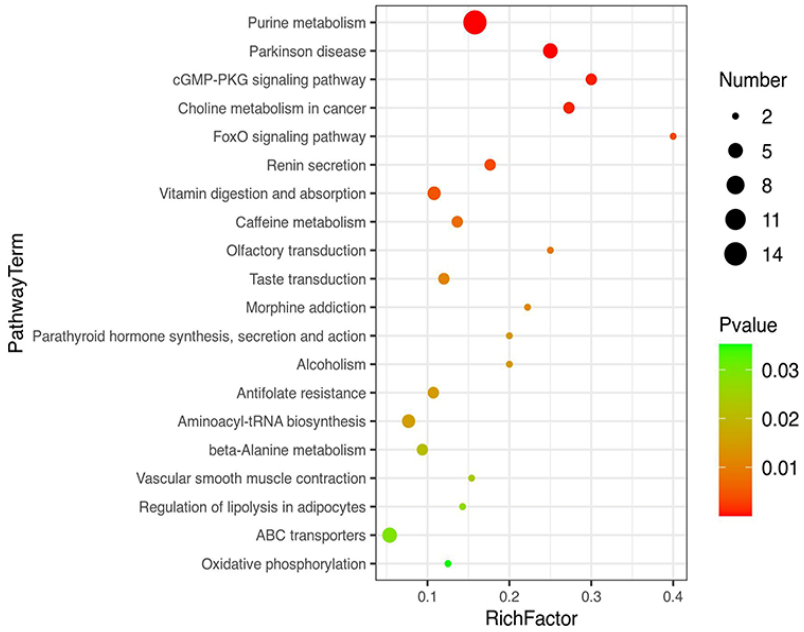

Figure 15. Bubble map of metabolic pathway.

Correlation between clinicopathological parameters and metabolites

We analyzed the relationships between biochemical and pathological indicators and the identified renal metabolites using Spearman or Pearson correlation **(Figure 16)**. The urinary albumin-to-creatinine ratio (UACR) showed significant associations with a range of metabolites, including 11,12-Epoxyeicosatrienoic acid, adenosine, LysoPA (18:0/0:0), asymmetric dimethylarginine, indoleacrylic acid, LysoPE species (22:5/0:0 and 0:0/20:4), methacholine, N-arachidonoyl taurine, NAD, N-linoleoyl taurine, various phosphatidylcholines (PC) and phosphatidylethanolamines (PE), PG (18:2/0:0), PI (20:4/0:0), PS (16:0/0:0), tetrahydro-2-methyl-3-furanol, and all-trans-heptaprenyl diphosphate. In the correlation plot, red dots indicate positive correlations, while blue dots represent negative correlations.

Functionally, adenosine is involved in purine metabolism and NAD participates in mitochondrial energy regulation, both of which relate to oxidative stress and inflammation. Additional metabolites, including adenosine 3'-monophosphate, asymmetric dimethylarginine, guanosine, indoleacrylic acid, and N-linoleoyl taurine, are linked to inflammatory pathways [6, 30–33], whereas 11,12-epoxyeicosatrienoic acid, guanosine, adenosine, and adenosine 3'-monophosphate are primarily associated with oxidative stress [34–39]. To confirm the downstream biological consequences, we further assessed markers of inflammation and oxidative stress.

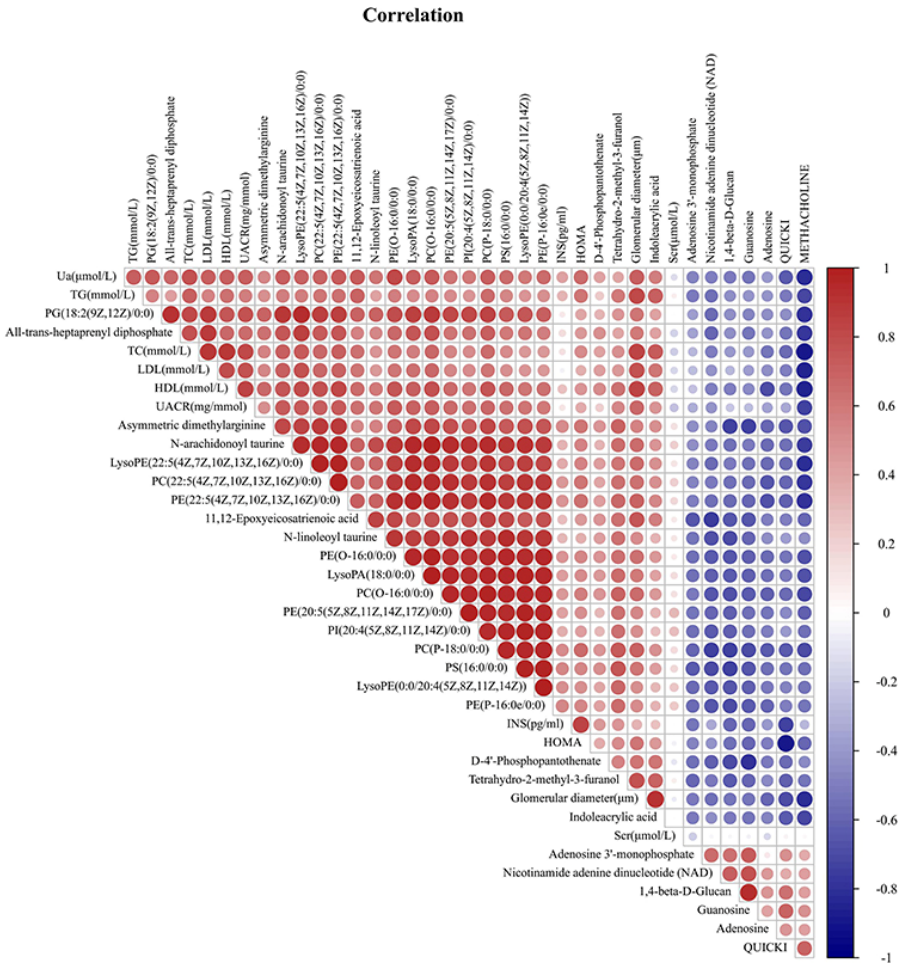

Figure 16. Heatmap showing correlations between clinicopathological parameters and identified renal metabolites.

Effect of semaglutide on inflammation and oxidative stress

To investigate whether semaglutide could restore the oxidative–antioxidative balance in obese mice, serum levels of SOD and MDA were measured. HFD-fed mice exhibited markedly lower SOD activity ($P < 0.001$) and elevated MDA levels ($P < 0.001$), reflecting heightened oxidative stress. Treatment with semaglutide significantly increased SOD activity ($P = 0.002$) and decreased renal MDA levels ($P = 0.001$), suggesting amelioration of oxidative–antioxidative imbalance.

We also assessed inflammatory markers in serum, including TNF-α, IL-6, and IL-1β. All three markers were significantly elevated in HFD mice, confirming the presence of systemic inflammation. Administration of semaglutide markedly reduced the levels of TNF-α, IL-6, and IL-1β ($P < 0.05$), indicating that semaglutide effectively suppresses the inflammatory response **(Figure 17)**.

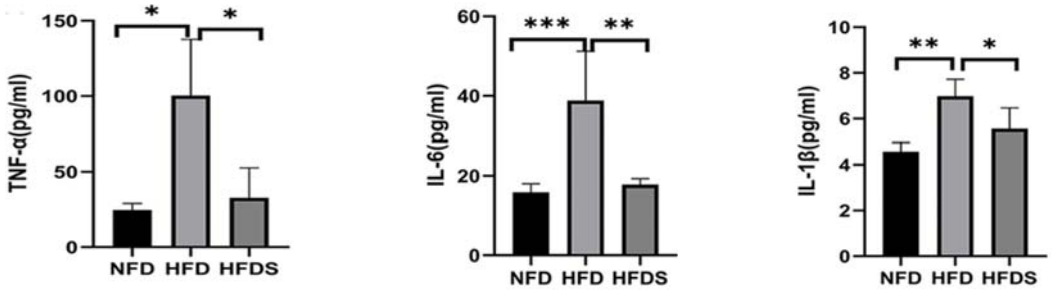

Figure 17. Semaglutide reduced HFD-induced inflammation and oxidative stress. Data represent mean ± SD for each group (n=8/group). *P<0.05, **P<0.01, ***P<0.001. (a) Serum TNF-α levels. (b) Serum IL-6 levels. (c) Serum IL-1β levels. (d) Serum SOD activity.

Obesity has emerged as a major global health challenge [4, 40–42]. Mounting evidence indicates that obesity independently elevates the risk of chronic kidney disease (CKD) progression [1, 3, 43, 44]. Glomerulopathy represents the predominant pathological feature of obesity-related kidney disease, where lipid accumulation in renal tissues triggers oxidative stress and activates pro-inflammatory pathways, ultimately causing podocyte injury, the central event driving obesity-related glomerulopathy (ORG) [5, 8, 13]. High-fat diet (HFD)-induced obesity in mice closely mimics human obesity pathophysiology. C57BL/6J mice, in particular, show heightened sensitivity to high-fat feeding, and feeding them an HFD for 8–16 weeks is widely used to establish the diet-induced obesity (DIO) model. These mice exhibit a systemic pro-inflammatory state akin to human metabolic syndrome, making them an ideal model for evaluating anti-obesity interventions [42, 43, 45].

Glucagon-like peptide-1 (GLP-1) is an incretin hormone secreted by intestinal cells, offering promising therapeutic potential for diabetes [5, 46]. Liraglutide, a clinically used GLP-1 analog, has a half-life of approximately 12 hours in humans [9–14]. Semaglutide, a more recently developed GLP-1 analog with a one-week half-life in humans, is modified at the eighth amino acid of liraglutide, enabling significant reductions in HbA1c and body weight. Semaglutide has received FDA approval for treating obesity with comorbidities [15, 16, 20, 47–50]. Studies have also demonstrated its cardiovascular protective effects, including attenuation of myocardial ischemia-reperfusion injury and infarction [16]. Due to the shorter half-life of semaglutide in rodents, daily dosing was employed in this study rather than the once-weekly regimen used in humans [17, 20, 49].

Metabolomics has emerged as a powerful tool for elucidating complex disease mechanisms by profiling biochemical signatures linked to pathogenesis and diagnosis. Unlike genomics, which may not always translate into functional outcomes, or proteomics, which may detect inactive proteins, metabolomics captures dynamic changes in small-molecule metabolites that reflect physiological alterations, providing amplified insight into systemic perturbations [8, 21–24, 51]. Notably, systematic metabolomic studies exploring semaglutide's effects on ORG have been limited.

In the present study, obese mice exhibited dyslipidemia and glucose metabolism disorders, whereas semaglutide treatment ameliorated insulin resistance, reduced lipid droplet accumulation, and alleviated glomerular and tubular injury, confirming its renal protective effects. Metabolomic analyses further elucidated the underlying mechanisms.

Phospholipids (PLs) and lysophospholipids (LysoPLs) play critical roles in cellular membranes and physiological processes. Phosphatidylcholine (PC) and phosphatidylethanolamine (PE), for example, are linked to cholesterol homeostasis and renal function [25, 52]. LysoPLs, produced by phospholipase A-mediated deacylation of PLs, include lysophosphatidic acid (LysoPA), lysophosphatidylcholine (LysoPC), lysophosphatidylethanolamine (LysoPE), lysophosphatidylglycerol (LysoPG), lysophosphatidylinositol (LysoPI), and lysophosphatidylserine (LysoPS). Their biological activities are diverse, and they are implicated in pathologies such as kidney injury, obesity, non-alcoholic fatty liver disease, and cancer. LysoPC, the most abundant LysoPL in human plasma, modulates vascular endothelial function, immune responses, and insulin secretion, while LysoPEs can activate MAPK signaling and exert neurotrophic effects [26, 47, 53]. In HFD mice, kidney levels of PLs and LysoPLs were markedly elevated, indicating lipid metabolic imbalance, which semaglutide treatment effectively mitigated.

Purinergic signaling, involving ATP and its degradation product adenosine, regulates renal water and sodium homeostasis, glomerular and tubular functions, and blood flow autoregulation. Adenosine acts as a paracrine anti-

inflammatory mediator by activating four G protein-coupled adenosine receptors (A1AR, A2AAR, A2BAR, A3AR), which inhibit macrophage activation and inflammatory cytokine production, including IL-6 and TGF-β1, while also modulating glucose clearance [6, 34, 37, 54, 55]. In this study, adenosine levels were reduced in obese mice but restored following semaglutide administration, suggesting its role in mitigating inflammation and improving renal function.

Nicotinamide adenine dinucleotide (NAD) is essential for mitochondrial electron transport, oxidative phosphorylation, and cellular energy metabolism. Both oxidized (NAD+) and reduced (NADH) forms are crucial for maintaining cellular redox balance [36, 56]. Declines in NAD+ are associated with aging, metabolic disorders, diabetes, and kidney injury. Recent studies highlight NAD+ as a key regulator of renal health, with impaired NAD+ biosynthesis exacerbating kidney injury [35, 36, 56, 57]. In HFD mice, NAD and taurine levels, critical for mitochondrial antioxidant defenses, were altered, and transmission electron microscopy revealed mitochondrial structural damage. Semaglutide treatment restored these metabolite levels and improved mitochondrial morphology, indicating enhanced renal mitochondrial function.

Our findings demonstrated that obese mice exhibited impaired glucose tolerance and insulin resistance. Among the metabolites identified in this study, four were associated with insulin resistance: cholic acid, 5-l-glutamyl-taurine, glucosamine, and suberic acid [29]. As the VIP scores of 5-l-glutamyl-taurine, glucosamine, and suberic acid were below 1, we did not pursue in-depth analyses of these three metabolites. Although cholic acid showed a P-value below 0.05, the differences among groups only displayed a trend. Previous research has indicated that insulin resistance correlates with reduced levels of cholic acid, deoxycholic acid, and their conjugates [29, 58], and supplementation of high-fat diets with cholic acid or chenodeoxycholic acid can attenuate obesity development in mice [55]. Our results align with these findings, supporting the role of cholic acid in insulin sensitivity.

Urinary albumin-to-creatinine ratio (UACR) is a key indicator of renal injury and dysfunction. Correlation analysis between UACR and identified metabolites may help screen potential biomarkers [22, 59]. Strong negative correlations between adenosine and NAD with UACR suggest that nucleotide and energy metabolism are intimately linked with ORG pathogenesis, indicating that these metabolites could serve as therapeutic targets. Guided by these metabolic findings, we further assessed inflammatory and oxidative stress markers.

Pro-inflammatory cytokines, including IL-1β and IL-6, play crucial roles in mediating inflammation, while TNF-α can amplify inflammatory cascades and is associated with obesity and insulin resistance [3, 16, 21, 32, 60]. In our study, semaglutide treatment significantly lowered the levels of IL-6, IL-1β, and TNF-α, demonstrating its anti-inflammatory effect. Oxidative stress promotes reactive oxygen species accumulation and lipid peroxidation, generating malondialdehyde (MDA) and causing cellular damage, whereas superoxide dismutase (SOD) functions as a key antioxidant enzyme to neutralize free radicals [16, 21]. Oil-red O staining revealed that semaglutide markedly reduced lipid accumulation in renal tissue, restoring the balance between oxidative and antioxidative processes. These findings are consistent with prior reports showing that semaglutide can improve cardiomyopathy and neurological disorders by mitigating inflammation and oxidative stress [15–17].

Overall, this study highlights the renoprotective effects of semaglutide in obese mice, as revealed by metabolomics. Nonetheless, there are some limitations. Additional experiments are necessary to determine the precise origins of key metabolites and the detailed pathways involved. Future studies will focus on mechanistic investigations at the cellular level, using targets identified through renal metabolomics.

Conclusion

In conclusion, metabolomic analyses provide novel insights into the mechanisms underlying semaglutide's renoprotective effects in ORG. The protective actions appear to involve phospholipid and lysophospholipid metabolism, purine metabolism, NAD metabolism, and insulin resistance-related metabolic pathways. These results suggest that semaglutide represents a promising therapeutic strategy for obesity-associated CKD.

Abbreviations

CKD, chronic kidney disease; ORG, obesity-related glomerulopathy; GLP-1, glucagon-like peptide-1; HFD, high-fat diet; Scr, serum creatinine; Ua, uric acid; TG, triglyceride; TC, total cholesterol; HDL, high-density lipoprotein; LDL, low-density lipoprotein; SOD, superoxide dismutase; MDA, malondialdehyde; IL-1β, interleukin-1β; IL-6, interleukin-6; TNF-α, tumor necrosis factor-α; NFD, normal-fat diet; UACR, urinary albumin/creatinine ratio; HOMA, homeostasis model assessment; QUICKI, Quantitative Insulin Sensitivity

index; Ccr, creatinine clearance; HE, hematoxylin and eosin; PAS, periodic acid-Schiff; TEM, transmission electron microscopy; PCA, Principle Component Analysis; OPLS-DA, Orthogonal Partial Least-Squares-Discriminant Analysis; RER, rough endoplasmic reticulum; PLs, phospholipids; LysoPLs, lysophospholipids; NAD, nicotinamide adenine dinucleotide.

Acknowledgments: None

Conflict of Interest: None

Financial Support: None

Ethics Statement: None

References

1. Gadde KM, Martin CK, Berthoud HR, Heymsfield SB, Fineman MS, Ravussin E, et al. Obesity: pathophysiology and management. J Am Coll Cardiol. 2018;71(1):69-84.
2. Andres-Hernando A, Lanaspa MA, Kuwabara M, Cicerchi C, Li N, Roncal-Jimenez CA, et al. Obesity causes renal mitochondrial dysfunction and energy imbalance and accelerates chronic kidney disease in mice. Am J Physiol Renal Physiol. 2019;317(4):F941-8.
3. Declèves AE, Sharma K. Obesity and kidney disease: differential effects of obesity on adipose tissue and kidney inflammation and fibrosis. Curr Opin Nephrol Hypertens. 2015;24(1):28-36.
4. McPherson KC, Shields CA, Poudel B, Barboza E, Opperman L, King KB, et al. Impact of obesity as an independent risk factor for the development of renal injury: implications from rat models of obesity. Am J Physiol Renal Physiol. 2019;316(2):F316-27.
5. Guo H, Wang B, Li H, Ling L, Niu J, Gu Y, et al. Glucagon-like peptide-1 analog prevents obesity-related glomerulopathy by inhibiting excessive autophagy in podocytes. Am J Physiol Renal Physiol. 2018;314(2):F181-9.
6. Zhu JJ, Chen YP, Yang M, Liu YF, Zhao LL, Lu K, et al. Aldosterone is involved in the pathogenesis of obesity-related glomerulopathy through activation of Wnt/β-catenin signaling in podocytes. Mol Med Rep. 2018;17(3):4589-98.
7. Hsu WC, Lin CS, Chen JF, Chen YC, Lee CC, Lin CH, et al. The effects of dipeptidyl peptidase 4 inhibitors on renal function in patients with type 2 diabetes mellitus. J Clin Med. 2022;11(9):2653.
8. Kuwahara S, Hosojima M, Kaneko R, Aoki H, Kabasawa H, Saito A, et al. Megalin-mediated tubuloglomerular alterations in high-fat diet-induced kidney disease. J Am Soc Nephrol. 2016;27(7):1996-2008.
9. Zhou JY, Poudel A, Welchko R, Mekala N, Griffin M, Threeton C, et al. Liraglutide improves insulin sensitivity in high fat diet induced diabetic mice through multiple pathways. Eur J Pharmacol. 2019;861:172594.
10. Le TD, Nguyen NPT, Nguyen ST, Tran VQ, Tran HTT, Nguyen TH, et al. The association between femoral artery intima-media thickness and serum glucagon-like peptide-1 levels among newly diagnosed patients with type 2 diabetes mellitus. Diabetes Metab Syndr Obes. 2020;13:3561-70.
11. Sheikh A. Direct cardiovascular effects of glucagon like peptide-1. Diabetol Metab Syndr. 2013;5:47.
12. Le TD, Nguyen NPT, Tran HTT, Nguyen ST, Tran VQ, Nguyen TH, et al. Diabetic peripheral neuropathy associated with cardiovascular risk factors and glucagon-like peptide-1 concentrations among newly diagnosed patients with type 2 diabetes mellitus. Diabetes Metab Syndr Obes. 2022;15:35-44.
13. Li K, Sun J, Huang N, Yang J, Xu J, Wang Y, et al. Liraglutide improves obesity-induced renal injury by alleviating uncoupling of the glomerular VEGF-NO axis in obese mice. Clin Exp Pharmacol Physiol. 2020;47(12):1978-84.
14. Luo Y, Yang P, Li Z, Pan M, Liu C, Xu J, et al. Liraglutide improves non-alcoholic fatty liver disease in diabetic mice by modulating inflammatory signaling pathways. Drug Des Devel Ther. 2019;13:4065-74.
15. Zhang L, Zhang L, Li L, Jiang H, Huo L, Liu B, et al. Semaglutide is neuroprotective and reduces α-synuclein levels in the chronic MPTP mouse model of Parkinson's disease. J Parkinsons Dis. 2019;9(1):157-71.

16. Li Q, Tuo X, Li B, Deng Z, Li Y, Liu X, et al. Semaglutide attenuates excessive exercise-induced myocardial injury through inhibiting oxidative stress and inflammation in rats. Life Sci. 2020;250:117531.
17. Basalay MV, Davidson SM, Yellon DM. Neuroprotection in rats following ischaemia-reperfusion injury by GLP-1 analogues-liraglutide and semaglutide. Cardiovasc Drugs Ther. 2019;33(6):661-7.
18. Pontes-da-Silva RM, de Souza Marinho T, de Macedo Cardoso LE, Andreotti L, Perini JA, de Oliveira TC, et al. Obese mice weight loss role on nonalcoholic fatty liver disease and endoplasmic reticulum stress treated by a GLP-1 receptor agonist. Int J Obes (Lond). 2022;46(1):21-9.
19. Rakipovski G, Rolin B, Nøhr J, Klewe I, Frederiksen KS, Augustin R, et al. The GLP-1 analogs liraglutide and semaglutide reduce atherosclerosis in ApoE(-/-) and LDLr(-/-) mice by a mechanism that includes inflammatory pathways. JACC Basic Transl Sci. 2018;3(6):844-57.
20. Lau J, Bloch P, Schäffer L, Pettersson I, Spetzler J, Kofoed J, et al. Discovery of the once-weekly glucagon-like peptide-1 (GLP-1) analogue semaglutide. J Med Chem. 2015;58(18):7370-80.
21. Liu J, Wang C, Liu F, Lu X, Li X, Wang L, et al. Metabonomics revealed xanthine oxidase-induced oxidative stress and inflammation in the pathogenesis of diabetic nephropathy. Anal Bioanal Chem. 2015;407(9):2569-79.
22. Wei T, Zhao L, Jia J, Xia W, Wang Y, Li Y, et al. Metabonomic analysis of potential biomarkers and drug targets involved in diabetic nephropathy mice. Sci Rep. 2015;5:11998.
23. Mulder S, Hammarstedt A, Nagaraj SB, Cummins C, Boucher J, Smith U, et al. A metabolomics-based molecular pathway analysis of how the sodium-glucose co-transporter-2 inhibitor dapagliflozin may slow kidney function decline in patients with diabetes. Diabetes Obes Metab. 2020;22(7):1157-66.
24. Chen H, Cao G, Chen DQ, Wang M, Vaziri ND, Zhao YY, et al. Metabolomics insights into activated redox signaling and lipid metabolism dysfunction in chronic kidney disease progression. Redox Biol. 2016;10:168-78.
25. Airaksinen K, Jokkala J, Ahonen I, Auriola S, Lehtonen M, Pihlajamäki J, et al. High-fat diet, betaine, and polydextrose induce changes in adipose tissue inflammation and metabolism in C57BL/6J mice. Mol Nutr Food Res. 2018;62(23):e1800455.
26. Cheng L, Zhang S, Shang F, Ning Y, Huang Z, He J, et al. Emodin improves glucose and lipid metabolism disorders in obese mice via activating brown adipose tissue and inducing browning of white adipose tissue. Front Endocrinol (Lausanne). 2021;12:618037.
27. Sun X, Han F, Lu Q, Li X, Ren D, Zhang J, et al. Empagliflozin ameliorates obesity-related cardiac dysfunction by regulating sestrin2-mediated AMPK-mTOR signaling and redox homeostasis in high-fat diet-induced obese mice. Diabetes. 2020;69(6):1292-305.
28. Wang D, Liu J, He S, Wang H, Hu Y, Sun H, et al. Assessment of early renal damage in diabetic rhesus monkeys. Endocrine. 2014;47(3):783-92.
29. Men L, Pi Z, Zhou Y, Zhang P, Liu Z, Liu Y, et al. Urine metabolomics of high-fat diet induced obesity using UHPLC-Q-TOF-MS. J Pharm Biomed Anal. 2017;132:258-66.
30. Ding S, Jiang H, Fang J, Liu Y, Zhang J, Zheng J, et al. Regulatory effect of resveratrol on inflammation induced by lipopolysaccharides via reprogramming intestinal microbes and ameliorating serum metabolism profiles. Front Immunol. 2021;12:777159.
31. Wlodarska M, Luo C, Kolde R, Xavier RJ, Kostic AD, Garrett WS, et al. Indoleacrylic acid produced by commensal peptostreptococcus species suppresses inflammation. Cell Host Microbe. 2017;22(1):25-37.
32. Luo Y, Chen H, Huang R, Wu Q, Li Y, He J, et al. Guanosine and uridine alleviate airway inflammation via inhibition of the MAPK and NF-κB signals in OVA-induced asthmatic mice. Pulm Pharmacol Ther. 2021;69:102049.
33. Huang S, Xu Y, Peng WF, Zhang J, Wang J, Wu C, et al. Asymmetric dimethylarginine targets MAPK pathway to regulate insulin resistance in liver by activating inflammation factors. J Cell Biochem. 2018;119(1):1-10.
34. Dwyer KM, Kishore BK, Robson SC. Conversion of extracellular ATP into adenosine: a master switch in renal health and disease. Nat Rev Nephrol. 2020;16(9):509-24.
35. Amjad S, Nisar S, Bhat AA, Shah AR, Frenneaux MP, Fakhro K, et al. Role of NAD(+) in regulating cellular and metabolic signaling pathways. Mol Metab. 2021;49:101195.
36. Faivre A, Katsyuba E, Verissimo T, Lythgoe H, Kaufmann P, Martinou JC, et al. Differential role of nicotinamide adenine dinucleotide deficiency in acute and chronic kidney disease. Nephrol Dial Transplant. 2021;36(1):60-8.

37. Pandey S, Aggarwal D, Gupta K, Yadav A, Kumar A, Singh P, et al. Adenosine an old player with new possibilities in kidney diseases: preclinical evidences and clinical perspectives. Life Sci. 2021;265:118834.
38. Liu T, Li T, Chen X, Zhang H, Liu J, Zhang X, et al. EETs/sEHi alleviates nociception by blocking the crosslink between endoplasmic reticulum stress and neuroinflammation in a central poststroke pain model. J Neuroinflammation. 2021;18(1):211.
39. Samala N, Tersey SA, Chalasani N, Anderson RM, Mirmira RG, Matherly SC, et al. Molecular mechanisms of nonalcoholic fatty liver disease: potential role for 12-lipoxygenase. J Diabetes Complications. 2017;31(11):1630-7.
40. Câmara NO, Iseki K, Kramer H, Wesson DE, Sharma K, Anders HJ, et al. Kidney disease and obesity: epidemiology, mechanisms and treatment. Nat Rev Nephrol. 2017;13(3):181-90.
41. Bovet P, Chiolero A, Gedeon J. Health effects of overweight and obesity in 195 countries. N Engl J Med. 2017;377(15):1495-6.
42. Wong SK, Chin KY, Suhaimi FH, Fairus A, Ima-Nirwana S. Animal models of metabolic syndrome: a review. Nutr Metab (Lond). 2016;13:65.
43. Mouton AJ, Li X, Hall ME, Hall JE, Wang Z, Li Y, et al. Obesity, hypertension, and cardiac dysfunction: novel roles of immunometabolism in macrophage activation and inflammation. Circ Res. 2020;126(6):789-806.
44. Carbone A, Al Salhi Y, Tasca A, Palleschi G, Fuschi A, De Nunzio C, et al. Obesity and kidney stone disease: a systematic review. Minerva Urol Nefrol. 2018;70(4):393-400.
45. Oh H, Jeong KH, Han HY, Lee MH, Kim HJ, Kim SH, et al. A potent and selective 11β-hydroxysteroid dehydrogenase type 1 inhibitor, SKI2852, ameliorates metabolic syndrome in diabetic mice models. Eur J Pharmacol. 2015;768:139-48.
46. Kim GW, Lin JE, Snook AE, Aing AS, Merlino DJ, Li P, et al. Calorie-induced ER stress suppresses uroguanylin satiety signaling in diet-induced obesity. Nutr Diabetes. 2016;6(5):e211.
47. Wang C, Li L, Liu S, Zhang Y, Wang X, Li X, et al. GLP-1 receptor agonist ameliorates obesity-induced chronic kidney injury via restoring renal metabolism homeostasis. PLoS One. 2018;13(3):e0193473.
48. Newsome PN, Buchholtz K, Cusi K, Linder M, Okanoue T, Ratziu V, et al. A placebo-controlled trial of subcutaneous semaglutide in nonalcoholic steatohepatitis. N Engl J Med. 2021;384(12):1113-24.
49. Nadolsky KZ, Agarwal M. Once-weekly semaglutide in adults with overweight or obesity. N Engl J Med. 2021;385(1):e4.
50. Zhang L, Zhang L, Li L, Jiang H, Huo L, Liu B, et al. Neuroprotective effects of the novel GLP-1 long acting analogue semaglutide in the MPTP Parkinson's disease mouse model. Neuropeptides. 2018;71:70-80.
51. Suh DH, Lee HW, Jung ES, Chae SW, Kong HJ, Kwon YD, et al. In vivo metabolomic interpretation of the anti-obesity effects of hyacinth bean (Dolichos lablab L.) administration in high-fat diet mice. Mol Nutr Food Res. 2017;61(8):1600895.
52. Shon JC, Kim WC, Ryu R, Yao Z, Kim JH, Kim ND, et al. Plasma lipidomics reveals insights into anti-obesity effect of chrysanthemum morifolium Ramat leaves and its constituent luteolin in high-fat diet-induced dyslipidemic mice. Nutrients. 2020;12(10):2973.
53. Yamamoto Y, Sakurai T, Chen Z, Furukawa T, Gowda SGN, Zhao H, et al. Analysis of serum lysophosphatidylethanolamine levels in patients with non-alcoholic fatty liver disease by liquid chromatography-tandem mass spectrometry. Anal Bioanal Chem. 2021;413(1):245-54.
54. Johnston-Cox H, Koupenova M, Yang D, Corkey B, Gokce N, Farb MG, et al. The A2b adenosine receptor modulates glucose homeostasis and obesity. PLoS One. 2012;7(7):e40584.
55. Pak ES, Jeong LS, Hou X, Kumar S, Lee JH, Choi WJ, et al. Dual actions of A(2A) and A(3) adenosine receptor ligand prevents obstruction-induced kidney fibrosis in mice. Int J Mol Sci. 2021;22(11):5667.
56. Covarrubias AJ, Perrone R, Grozio A, Verdin E. NAD(+) metabolism and its roles in cellular processes during ageing. Nat Rev Mol Cell Biol. 2021;22(2):119-41.
57. Liu X, Luo D, Huang S, Deng J, Wang Y, Shi L, et al. Impaired nicotinamide adenine dinucleotide biosynthesis in the kidney of chronic kidney disease. Front Physiol. 2021;12:723690.
58. Ippagunta SM, Kharitonenkov A, Adams AC, Rajapaksha TW, Flynn CR, et al. Cholic acid supplementation of a high-fat obesogenic diet suppresses hepatic triacylglycerol accumulation in mice via a fibroblast growth factor 21-dependent mechanism. J Nutr. 2018;148(4):510-7.

59. Li M, Wang X, Aa J, Yang M, Lu Y, Li J, et al. GC/TOFMS analysis of metabolites in serum and urine reveals metabolic perturbation of TCA cycle in db/db mice involved in diabetic nephropathy. Am J Physiol Renal Physiol. 2013;304(11):F1317-24.
60. Akash MSH, Rehman K, Liaqat A. Tumor necrosis factor-alpha: role in development of insulin resistance and pathogenesis of type 2 diabetes mellitus. J Cell Biochem. 2018;119(1):105-10.